

MEASUREMENT OF THE COSMIC MICROWAVE BACKGROUND BISPECTRUM ON THE *COBE* DMR SKY MAPS

E. Komatsu^{1,2}, B. D. Wandelt³, D. N. Spergel^{1,4}, A. J. Banday⁵, and K. M. Górski^{6,7}

ABSTRACT

We measure the angular bispectrum of the cosmic microwave background (CMB) radiation anisotropy from the *COBE* Differential Microwave Radiometer (DMR) four-year sky maps. The angular bispectrum is the harmonic transform of the three-point correlation function, analogous to the angular power spectrum, the harmonic transform of the two-point correlation function. First, we study statistical properties of the bispectrum and the *normalized* bispectrum. We find the latter more useful for statistical analysis; the distribution of the normalized bispectrum is very much Gaussian, while the bare bispectrum distribution is highly non-Gaussian. Then, we measure 466 modes of the normalized bispectrum, all independent combinations of three-point configurations up to a maximum multipole of 20, the mode corresponding to the DMR beam size. By measuring 10 times as many modes as the sum of previous work, we test Gaussianity of the DMR maps. We compare the data with the simulated Gaussian realizations, finding no significant detection of the normalized bispectrum on the mode-by-mode basis. We also find that the previously reported detection of the normalized bispectrum is consistent with a statistical fluctuation. By fitting a theoretical prediction to the data for the primary CMB bispectrum, which is motivated by slow-roll inflation, we put a weak constraint on a parameter characterizing non-linearity in inflation. Simultaneously fitting the foreground bispectra estimated from interstellar dust and synchrotron template maps shows that neither dust nor synchrotron emissions significantly contribute to the bispectrum at high Galactic latitude. We conclude that the DMR map is consistent with Gaussianity.

Subject headings: cosmology: observations – cosmic microwave background – early universe

¹Department of Astrophysical Sciences, Princeton University, Princeton, NJ 08544, USA

¹Astronomical Institute, Tôhoku University, Aoba, Sendai 980-8578, Japan

³Department of Physics, Princeton University, Princeton, NJ 08544, USA

⁴W. M. Keck Distinguished Visiting Professor, School of Natural Sciences, Institute for Advanced Study, NJ 08540, USA

⁵Max Planck Institut für Astrophysik, Karl Schwarzschild Strasse 1, D-85740 Garching bei München, Germany

⁶European Southern Observatory, Karl Schwarzschild Strasse 2, D-85740 Garching bei München, Germany

⁷Warsaw University Observatory, Aleje Ujazdowskie 4, 00-478 Warszawa, Poland

1. INTRODUCTION

Why study non-Gaussianity of the cosmic microwave background (CMB) radiation anisotropy?

Inflation (Guth 1981; Sato 1981; Albrecht and Steinhardt 1982; Linde 1982) predicts Gaussian primordial perturbations in quantum origin (Guth and Pi 1982; Hawking 1982; Starobinsky 1982; Bardeen et al. 1983), implying that two-point statistics such as the angular power spectrum, C_l , specify all the statistical properties of the CMB anisotropy. Inflation has passed several challenging observational tests; the recent CMB experiments (Miller et al. 1999; de Bernadis et al. 2000; Hanany et al. 2000) have shown that the universe is flat as predicted by inflation with a fluctuation spectrum consistent with an adiabatic scale-invariant fluctuation.

Several authors have attempted to measure non-Gaussianity in CMB using various statistical techniques (e.g., Kogut et al. 1996b); as yet no conclusive detection has been reported except for measurement of several modes of the normalized CMB bispectrum on the *COBE* Differential Microwave Radiometer (DMR) sky maps (Ferreira et al. 1998; Magueijo 2000). The existence of non-Gaussianity in the DMR data is controversial. If the CMB sky were non-Gaussian, this would challenge our simplest inflationary model.

The angular bispectrum, $B_{l_1 l_2 l_3}$, is the harmonic transform of the three-point correlation function. We carefully distinguish the normalized bispectrum, $B_{l_1 l_2 l_3} / (C_{l_1} C_{l_2} C_{l_3})^{1/2}$, from the bispectrum, $B_{l_1 l_2 l_3}$. Ferreira et al. (1998) have measured 9 equilateral ($l_1 = l_2 = l_3$) modes of the normalized bispectrum, $B_{l_1 l_2 l_3} / (C_{l_1} C_{l_2} C_{l_3})^{1/2}$, on the DMR map, claiming detection at $l_1 = l_2 = l_3 = 16$. Their result has been under extensive efforts to confirm its significance and origin. Bromley and Tegmark (1999) claim that a few individual pixels in the DMR map are responsible for the most of the signal. Banday et al. (2000) have proposed an eclipse effect by the Earth against the *COBE* satellite as a possible source of the signal. Magueijo (2000) has measured other 8 inter- l modes of the normalized bispectrum such as $B_{l-1 l l+1} / (C_{l-1} C_l C_{l+1})^{1/2}$, and claims that scatter of the normalized bispectrum among 8 modes is too small to be consistent with Gaussian. Sandvik and Magueijo (2000) further report measurement of 24 other inter- l modes for different lags in l , and conclude they are consistent with Gaussian.

Hence, until now 41 modes of the normalized bispectrum have been measured on the DMR map. Here, we simply ask: “how many modes are available in the DMR map for the bispectrum?” The answer is 466, up to a maximum multipole of 20 that corresponds to the DMR beam size; thus, it is conceivable that the claimed detection of the normalized bispectrum at $l_1 = l_2 = l_3 = 16$ would be explained by a statistical fluctuation, as 9 modes are expected to have statistical significance above 98% out of 466 independent modes even if CMB is exactly Gaussian. In this paper, we measure 466 modes of the CMB bispectrum on the *COBE* DMR sky maps, testing the claimed detection of the bispectrum and non-Gaussianity. We take into account the covariance between these modes due to the Galactic cut, which has not been done in the previous work.

On the theoretical side, several predictions for the CMB bispectrum exist. Several authors (Falk

et al. 1993; Luo and Schramm 1993; Gangui et al. 1994) have predicted the primary bispectrum (or equivalently three-point correlation function) on the DMR angular scales from slow-roll inflation models. Komatsu and Spergel (2001) have extended the prediction down to arcminutes scales using the full radiation transfer function.

In addition to the primary one, secondary sources in the low-redshift universe and foreground sources produce the bispectrum through their non-linearity. Luo and Schramm (1993) and Spergel and Goldberg (1999) have calculated the secondary bispectrum arising from non-linear evolution of gravitational potential; Goldberg and Spergel (1999) and Cooray and Hu (2000) have calculated the one from the gravitational lensing effect coupled with various secondary anisotropy sources. Komatsu and Spergel (2001) have calculated the foreground bispectrum from extragalactic radio and infrared point sources. While the bispectrum is not the best tool for detecting the signature of rare highly non-linear events, e.g., textures (Phillips and Kogut 2001), it is sensitive to weakly non-linear effects.

Having theoretical predictions is a great advantage in extracting physical information from measurement; one can fit a predicted bispectrum to the data so as to constrain parameters in a theory. Since the DMR beam size is large enough to minimize contribution from the secondary and the extragalactic foreground sources, the only relevant source would be the primary one. In this paper, we fit a theoretical primary bispectrum (Komatsu and Spergel 2001) to the data.

The Galactic plane contains strong microwave emissions from interstellar sources. The emissions are highly non-Gaussian, and distributed on fairly large angular scales. Unfortunately, predicting the CMB bispectrum from interstellar sources is very difficult; thus, we excise the galactic plane from the DMR data. We model the residual foreground bispectrum at high galactic latitude using foreground template maps. By simultaneously fitting the foreground bispectrum and the primary bispectrum to the DMR data for three different Galactic cuts, we quantify the importance of the interstellar emissions in our analysis.

This paper is organized as follows. In § 2, we define the angular bispectrum, and show how to compute it efficiently from observational data. In § 3, we study statistical properties of the bispectrum and the normalized bispectrum. We then measure the normalized bispectrum on the *COBE* DMR four-year sky maps (Bennett et al. 1996), testing Gaussianity of the DMR map. In § 4, we fit predicted bispectra to the DMR data, constraining parameters in the predictions. The predictions include the primary bispectrum from inflation and the foreground bispectrum from interstellar Galactic emissions. Finally, § 5 concludes. In the appendix, we derive the relations between the angular power spectrum and bispectrum on the incomplete sky and those on the full sky.

2. ANGULAR BISPECTRUM

The CMB angular bispectrum consists of a product of three harmonic transforms of the CMB temperature field. For Gaussian fields, expectation value of the bispectrum is exactly zero. Given statistical isotropy of the universe, the angular averaged bispectrum, $B_{l_1 l_2 l_3}$, is given by

$$B_{l_1 l_2 l_3} = \sum_{\text{all } m} \begin{pmatrix} l_1 & l_2 & l_3 \\ m_1 & m_2 & m_3 \end{pmatrix} a_{l_1 m_1} a_{l_2 m_2} a_{l_3 m_3}, \quad (1)$$

where the matrix denotes the Wigner-3j symbol. The harmonic coefficients, a_{lm} , are given by

$$a_{lm} = \int_{\Omega_{\text{obs}}} d^2 \hat{\mathbf{n}} \frac{\Delta T(\hat{\mathbf{n}})}{T} Y_{lm}^*(\hat{\mathbf{n}}), \quad (2)$$

where Ω_{obs} denotes a solid angle of the observed sky. $B_{l_1 l_2 l_3}$ satisfies the triangle condition, $|l_i - l_j| \leq l_k \leq l_i + l_j$ for all permutations of indices, and parity invariance, $l_1 + l_2 + l_3 = \text{even}$.

We rewrite equation (1) into a more computationally efficient form. Using the identity,

$$\begin{aligned} \begin{pmatrix} l_1 & l_2 & l_3 \\ m_1 & m_2 & m_3 \end{pmatrix} &= \begin{pmatrix} l_1 & l_2 & l_3 \\ 0 & 0 & 0 \end{pmatrix}^{-1} \sqrt{\frac{(4\pi)^3}{(2l_1 + 1)(2l_2 + 1)(2l_3 + 1)}} \\ &\times \int \frac{d^2 \hat{\mathbf{n}}}{4\pi} Y_{l_1 m_1}(\hat{\mathbf{n}}) Y_{l_2 m_2}(\hat{\mathbf{n}}) Y_{l_3 m_3}(\hat{\mathbf{n}}), \end{aligned} \quad (3)$$

we rewrite equation (1) as

$$B_{l_1 l_2 l_3} = \begin{pmatrix} l_1 & l_2 & l_3 \\ 0 & 0 & 0 \end{pmatrix}^{-1} \int \frac{d^2 \hat{\mathbf{n}}}{4\pi} e_{l_1}(\hat{\mathbf{n}}) e_{l_2}(\hat{\mathbf{n}}) e_{l_3}(\hat{\mathbf{n}}), \quad (4)$$

where the integral is not over Ω_{obs} , but over the whole sky; $e_l(\hat{\mathbf{n}})$ already encapsulates the information of incomplete sky coverage through a_{lm} . Here, following Spergel and Goldberg (1999), we have used the azimuthally averaged harmonic transform of the CMB temperature field, $e_l(\hat{\mathbf{n}})$,

$$e_l(\hat{\mathbf{n}}) = \sqrt{\frac{4\pi}{2l + 1}} \sum_m a_{lm} Y_{lm}(\hat{\mathbf{n}}). \quad (5)$$

Similarly, we write the angular power spectrum, C_l , as

$$C_l = \int \frac{d^2 \hat{\mathbf{n}}}{4\pi} e_l^2(\hat{\mathbf{n}}). \quad (6)$$

$e_l(\hat{\mathbf{n}})$ is thus a square-root of C_l at a given position of the sky.

Equation (4) is computationally efficient, as we can calculate $e_l(\hat{\mathbf{n}})$ quickly with the spherical harmonic transform for a given l . Since the HEALPix pixels have the equal area (Górski et al. 1998), the average over the whole sky, $\int d^2 \hat{\mathbf{n}} / (4\pi)$, is done by the sum over all pixels divided by the total number of pixels, $N^{-1} \sum_i^N$.

3. MEASUREMENT OF BISPECTRUM ON THE *COBE* DMR SKY MAPS

3.1. The data

We use the HEALPix-formatted (Górski et al. 1998) *COBE* DMR four-year sky map, which contains 12,288 pixels in Galactic coordinate with a pixel size $1^\circ 83$. We obtain the most sensitive sky map to CMB by combining 53 GHz map with 90 GHz map, after coadding the channels A and B at each frequency. We do not subtract eclipse season time-ordered data; while Banday et al. (2000) ascribe the reported non-Gaussianity to this data, we will argue in this paper that the claimed detection of the normalized bispectrum at $l_1 = l_2 = l_3 = 16$ (Ferreira et al. 1998) can also be explained in terms of a statistical fluctuation.

We reduce interstellar Galactic emissions by using three different Galactic cuts: the 20° cut, the extended cut (Banday et al. 1997), and the 25° cut. We then subtract the monopole and the dipole from each cut map, minimizing contaminations from these two multipoles to higher order multipoles through the mode-mode coupling. The coupling arises from incomplete sky coverage. This is very important to do, for the leakage of power from the monopole and the dipole to the higher order multipoles is rather big. We use the least-squares fit weighted by the pixel noise variance to measure the monopole and the dipole on each cut map.

We measure the bispectrum, $B_{l_1 l_2 l_3}$, on the DMR sky maps as follows. First, we measure a_{lm} using equation (2). Then, we transform a_{lm} for $-l \leq m \leq l$ into $e_l(\hat{\mathbf{n}})$ through equation (5). Finally, we obtain $B_{l_1 l_2 l_3}$ from equation (4), arranging l_1 , l_2 , and l_3 in order of $l_1 \leq l_2 \leq l_3$, where we set the maximum l_3 to be 20. In total, we have 466 non-zero modes after taking into account $|l_i - l_j| \leq l_k \leq l_i + l_j$ and $l_1 + l_2 + l_3 = \text{even}$. Measurement of 466 modes takes about 1 second of CPU time on a Pentium-III single processor personal computer.

3.2. Monte–Carlo Simulations

We use Monte–Carlo simulations to estimate the covariance matrix of the measured bispectrum. Our simulation includes (a) a Gaussian random realization of the primary CMB anisotropy field drawn from the *COBE*-normalized Λ CDM power spectrum, and (b) a Gaussian random realization of the instrumental noise drawn from diagonal terms of the *COBE* DMR noise covariance matrix (Lineweaver et al. 1994). For computational efficiency, we do not use off-diagonal terms as they are smaller than 1% of the diagonal terms (Lineweaver et al. 1994).

We generate the input power spectrum, C_l , using the CMBFAST code (Seljak and Zaldarriaga 1996) with cosmological parameters fixed at $\Omega_{\text{cdm}} = 0.25$, $\Omega_\Lambda = 0.7$, $\Omega_b = 0.05$, $h = 0.7$, and $n = 1$; the CMBFAST code uses the Bunn and White (1997) power-spectrum normalization.

In each realization, we generate a_{lm} from the power spectrum, multiply it by the harmonic-transformed DMR beam, G_l (Wright et al. 1994), transform $G_l a_{lm}$ back to a sky map, and add an

instrumental noise realization to the map. Finally, we measure 466 modes of the bispectrum from each realization. We generate 50,000 realizations for one simulation; processing one realization takes about 1 second, so that one simulation takes about 16 hours of CPU time on a Pentium-III single processor personal computer.

3.3. Normalized bispectrum

The input power spectrum determines the variance of the bispectrum. Off-diagonal terms in the covariance matrix arise from incomplete sky coverage. When non-Gaussianity is weak, the variance is given by (Luo 1994; Heavens 1998; Spergel and Goldberg 1999; Gangui and Martin 2000)

$$\langle B_{l_1 l_2 l_3}^2 \rangle = \langle C_{l_1} \rangle \langle C_{l_2} \rangle \langle C_{l_3} \rangle \Delta_{l_1 l_2 l_3}, \quad (7)$$

where $\Delta_{l_1 l_2 l_3}$ takes values 1, 2, or 6 for all l 's are different, two are same, or all are same, respectively. The brackets denote the ensemble average.

The variance is undesirably sensitive to the input power spectrum; even if the input power spectrum were slightly different from the true power spectrum on the DMR map, the estimated variance from simulations would be significantly wrong, and we would erroneously conclude that the DMR map is inconsistent with Gaussian. It is thus not a robust test of Gaussianity to compare the measured bispectrum with the Monte–Carlo simulations.

The *normalized* bispectrum, $B_{l_1 l_2 l_3} / (C_{l_1} C_{l_2} C_{l_3})^{1/2}$, is more sensible quantity than the bare bispectrum. Magueijo (1995) shows that the normalized bispectrum is a rotationally invariant spectrum independent of the power spectrum, as it factors out fluctuation amplitude in a_{lm} , which is measured by $C_l^{1/2}$. By construction, the variance of the normalized bispectrum is insensitive to the power spectrum, approximately given by $\Delta_{l_1 l_2 l_3}$.

One might wonder if the normalized bispectrum is too noisy to be useful, as the power spectrum in the denominator is also uncertain; however, we find that the variance is actually slightly smaller than $\Delta_{l_1 l_2 l_3}$. Figure 1 compares the variance of the normalized bispectrum, $\langle B_{l_1 l_2 l_3}^2 / (C_{l_1} C_{l_2} C_{l_3}) \rangle$, with that of the bispectrum, $\langle B_{l_1 l_2 l_3}^2 \rangle / (\langle C_{l_1} \rangle \langle C_{l_2} \rangle \langle C_{l_3} \rangle)$. The top-left panel shows the case of full sky coverage. We find that the variance of the normalized bispectrum is precisely 1 when all l 's are different, while it is slightly smaller than 2 or 6 when two l 's are same or all l 's are same, respectively. This arises due to correlation between the uncertainties in the bispectrum and the power spectrum, and this correlation tends to reduce the total variance of the normalized bispectrum. The rest of panels show the cases of incomplete sky coverage. While the variance becomes more scattered than the case of full sky coverage, the variance of the normalized bispectrum is still systematically smaller than that of the bare bispectrum. The normalized bispectrum is thus reasonably sensitive to non-Gaussianity, yet it is not sensitive to the overall normalization of power spectrum.

What distribution does the normalized bispectrum obey for a Gaussian field? First, even for a

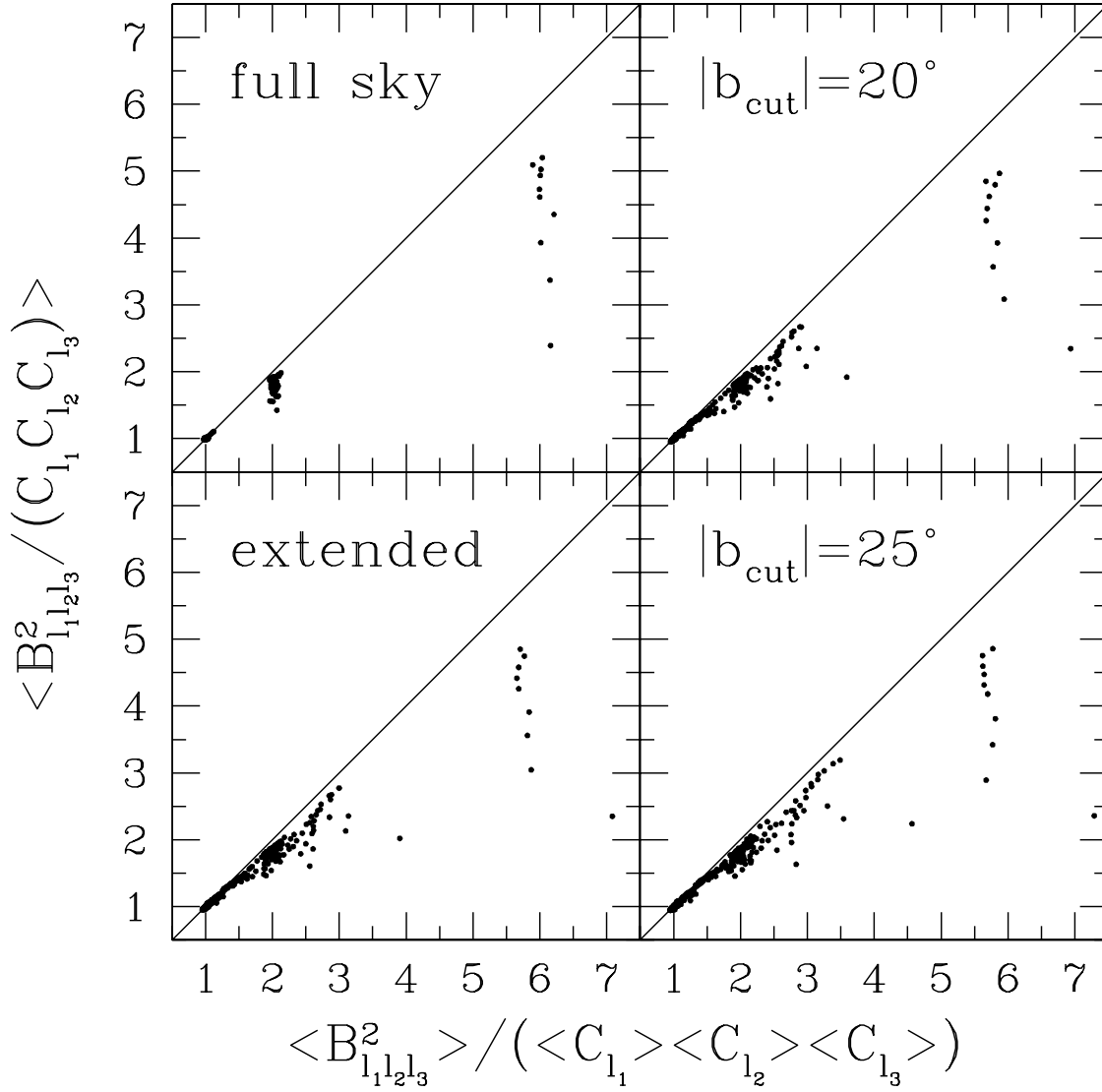


Fig. 1.— Comparison of the variance of the normalized bispectrum, $\langle B_{l_1 l_2 l_3}^2 / (C_{l_1} C_{l_2} C_{l_3}) \rangle$, with that of the bare bispectrum, $\langle B_{l_1 l_2 l_3}^2 \rangle / (\langle C_{l_1} \rangle \langle C_{l_2} \rangle \langle C_{l_3} \rangle)$. The top-left panel shows the case of full sky coverage, while the rest of panels show the cases of incomplete sky coverage. The top-right, bottom-left, and bottom-right panels use the 20° cut, the extended cut, and the 25° cut, respectively.

Gaussian field, the probability distribution of a single mode of $B_{l_1 l_2 l_3}$ is non-Gaussian, characterized by a large kurtosis. Figure 2 plots the distributions of 9 modes of $B_{l_1 l_2 l_3}$ drawn from the Monte–Carlo simulations (solid lines) in comparison with Gaussian distributions calculated from r.m.s. values (dashed lines). We find that the distribution does not fit the Gaussian very well. Then, we examine distribution of the normalized bispectrum, $B_{l_1 l_2 l_3} / (C_{l_1} C_{l_2} C_{l_3})^{1/2}$. We find that the distribution is very much Gaussian except for $l_1 = l_2 = l_3 = 2$. Figure 3 plots the distributions of the 9 modes of the normalized bispectrum (solid lines) in comparison with Gaussian distributions calculated from r.m.s. values (dashed lines). The distribution fits the Gaussian remarkably well; this motivates our using standard statistical methods developed for Gaussian fields to analyze the normalized bispectrum. We could not make this simplification if we were analyzing the bare bispectrum. Furthermore, the central limit theorem implies that when we combine 466 modes the deviation of the distribution from Gaussianity becomes even smaller.

Ferreira et al. (1998) claim detection of the normalized bispectrum at $l_1 = l_2 = l_3 = 16$; Magueijo (2000) claims that the scatter of the normalized bispectrum for $l_1 = l_2 - 1$ and $l_3 = l_2 + 1$ is too small to be consistent with Gaussian. The former has analyzed 9 modes, while the latter has analyzed 8 modes. In the next section, we analyze 466 modes, testing the statistical significance of the non-Gaussianity with much more samples than the previous work. We calculate C_l from equation (6), and then divide $B_{l_1 l_2 l_3}$ by $(C_{l_1} C_{l_2} C_{l_3})^{1/2}$ to obtain the normalized bispectrum.

3.4. Testing Gaussianity of the DMR map

We characterize statistical significance of the normalized bispectrum as probability of the measured normalized bispectrum being greater than those drawn from the Monte–Carlo simulations. We define the probability P as

$$P_\alpha \equiv \frac{N(|I_\alpha^{\text{DMR}}| > |I_\alpha^{\text{MC}}|)}{N_{\text{total}}} = \int_{-|I_\alpha^{\text{DMR}}|}^{|I_\alpha^{\text{DMR}}|} dx F_\alpha^{\text{MC}}(x), \quad (8)$$

where I_α is the normalized bispectrum, $N_{\text{total}} = 50,000$ is the total number of simulated realizations, and $\alpha = 1, 2, 3, 4, \dots, 466$ represent $(l_1, l_2, l_3) = (2, 2, 2), (2, 3, 3), (2, 2, 4), (3, 3, 4), \dots, (20, 20, 20)$, respectively, with satisfying $l_1 \leq l_2 \leq l_3$, $|l_i - l_j| \leq l_k \leq l_i + l_j$, and $l_1 + l_2 + l_3 = \text{even}$. $F_\alpha^{\text{MC}}(x)$ is the p.d.f of the simulated realizations for the normalized bispectrum, $x = I_\alpha^{\text{MC}}$. The p.d.f is normalized to unity: $\int_{-\infty}^{\infty} dx F_\alpha^{\text{MC}}(x) = 1$; thus, P_α lies in $0 \leq P_\alpha \leq 1$.

By construction, the distribution of P_α is uniform, if the DMR map is consistent with the simulated realizations, i.e., Gaussian. We give the proof as follows. By rewriting equation (8) as $P_\alpha = f(|I_\alpha^{\text{DMR}}|)$, we calculate the p.d.f of P_α , $G(P_\alpha)$, as

$$\begin{aligned} G(P_\alpha) &= \int_{-\infty}^{\infty} dy \delta [P_\alpha = f(|y|)] F_\alpha^{\text{DMR}}(y) \\ &= \int_0^{\infty} dy \delta [P_\alpha = f(y)] [F_\alpha^{\text{DMR}}(y) + F_\alpha^{\text{DMR}}(-y)] \end{aligned}$$

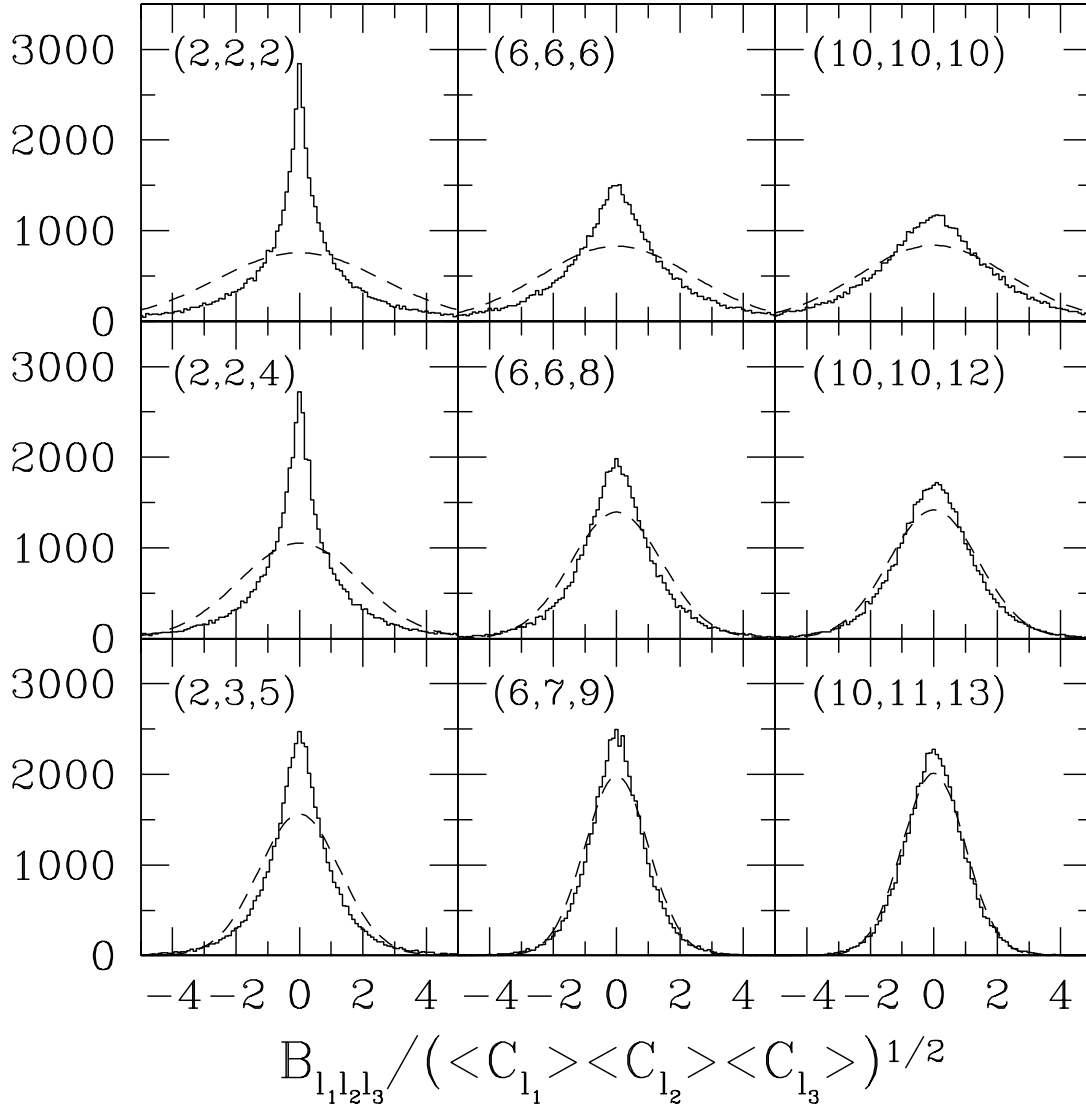


Fig. 2.— Distribution of the bispectrum drawn from the Monte–Carlo simulations for the 20° Galactic cut (solid lines). $B_{l_1 l_2 l_3} / (\langle C_{l_1} \rangle \langle C_{l_2} \rangle \langle C_{l_3} \rangle)^{1/2}$ is plotted, where the brackets denote the ensemble average over realizations from the Monte–Carlo simulations. The dashed lines plot Gaussian distributions calculated from r.m.s. values. Each panel represents a certain mode of (l_1, l_2, l_3) as quoted in the panels.

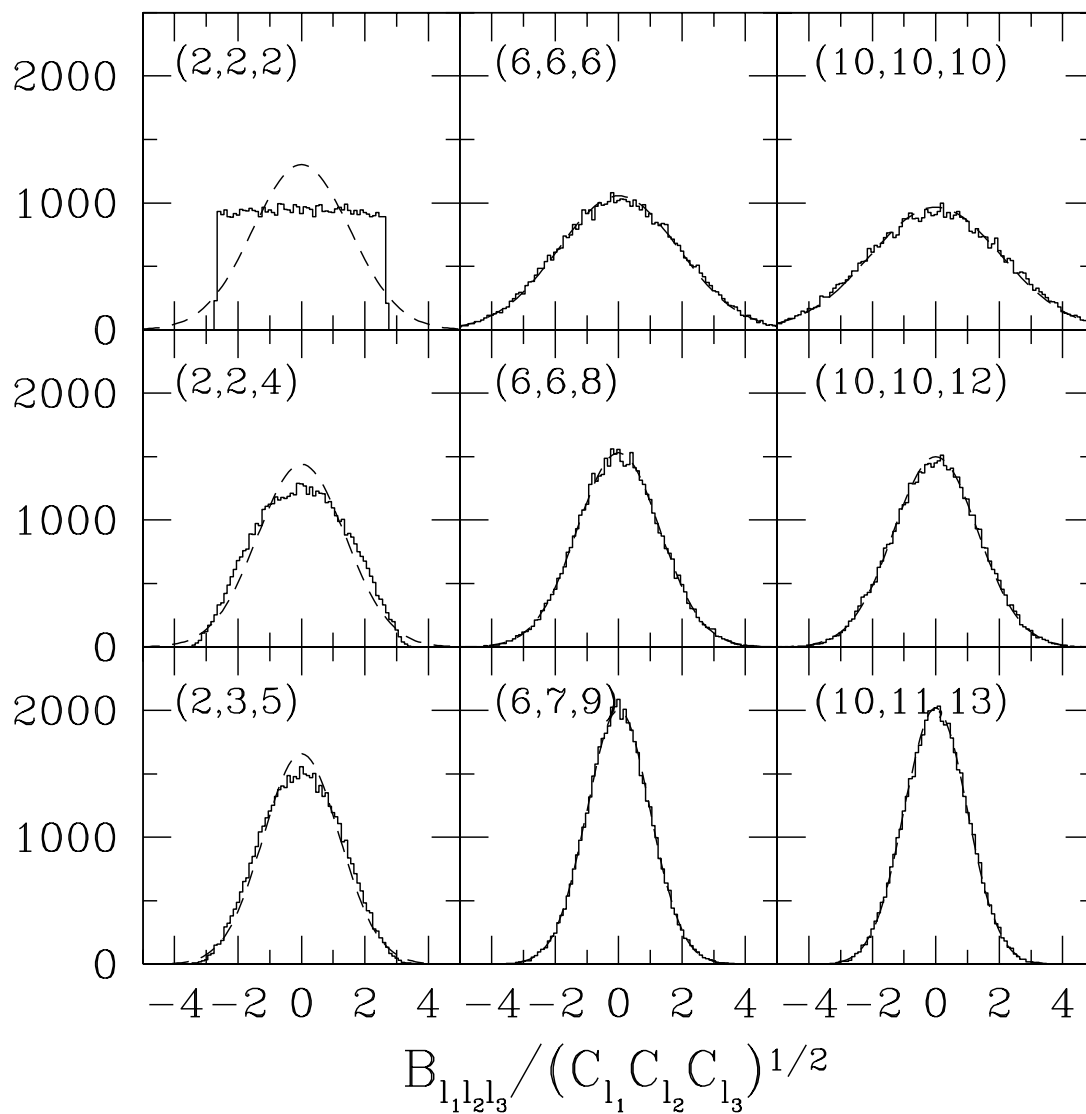


Fig. 3.— Distribution of the normalized bispectrum, $B_{l_1 l_2 l_3} / (C_{l_1} C_{l_2} C_{l_3})^{1/2}$, drawn from the Monte-Carlo simulations for the 20° Galactic cut. The meaning of the lines is the same as in figure 2.

$$\begin{aligned}
 &= \int_0^\infty dy \frac{\delta [y = f^{-1}(P_\alpha)]}{|df/dy|} [F_\alpha^{\text{DMR}}(y) + F_\alpha^{\text{DMR}}(-y)] \\
 &= \int_0^\infty dy \delta [y = f^{-1}(P_\alpha)] \frac{F_\alpha^{\text{DMR}}(y) + F_\alpha^{\text{DMR}}(-y)}{F_\alpha^{\text{MC}}(y) + F_\alpha^{\text{MC}}(-y)}, \tag{9}
 \end{aligned}$$

where $F_\alpha^{\text{DMR}}(y)$ is the p.d.f of the measured normalized bispectrum on the DMR map, $y = I_\alpha^{\text{DMR}}$. Our goal is to see if $F_\alpha^{\text{DMR}}(y)$ is consistent with the DMR data being Gaussian. It follows from equation (9) that $G(P_\alpha) \equiv 1$, when $F_\alpha^{\text{DMR}}(y) \equiv F_\alpha^{\text{MC}}(y)$, regardless of the functional form of $F_\alpha^{\text{MC}}(y)$. In other words, the distribution of P_α is uniform, if the distribution of the measured normalized bispectrum is the same as the simulated realizations. Since our simulation assumes the DMR map Gaussian, the P distribution, $G(P)$, tests Gaussianity of the DMR map. If the P distribution is not uniform, then we conclude the DMR data to be non-Gaussian.

A Gaussian field gives equal number of modes in each bin of P . For example, it gives 46.6 modes in $\Delta P = 10\%$ bin: $466 \times G(P) \Delta P = 466 \times 0.1 = 46.6$. If we detect the normalized bispectrum significantly, then we find that $G(P)$ is not uniform, but increases rapidly as P increases.

The top panel of figure 4 plots the P distribution for the three different Galactic cuts. We find that the distribution is uniform, and the number of modes in the bin ($\Delta P = 10\%$) is consistent with the expectation value for Gaussian fluctuations (46.6).

To further quantify how well it is uniform, we calculate the Kolmogorov–Smirnov (KS) statistic for the P distribution in comparison with the uniform distribution. The bottom panel of figure 4 plots the cumulative P distribution, for which we calculate the KS statistic. The probability of the distribution being uniform is 6.7%, 73%, and 77% for the three Galactic cuts, respectively.

We have confirmed that the normalized bispectrum at $l_1 = l_2 = l_3 = 16$ has $P = 97.81\%$ for the 20° cut, $P = 99.97\%$ for the extended cut, and $P = 99.27\%$ for the 25° cut, as similar to Ferreira et al. (1998); however, our result shows that statistical fluctuations explain the significance. We conclude that the properties of the normalized bispectrum of the DMR map are consistent with CMB being a Gaussian field.

4. MODEL FITTING

In this section, we fit predicted CMB bispectra to the measured normalized bispectrum. The predictions include the primary bispectrum from inflation and the interstellar foreground bispectrum from the Galactic emissions. Then, we constrain a parameter characterizing the primary bispectrum.

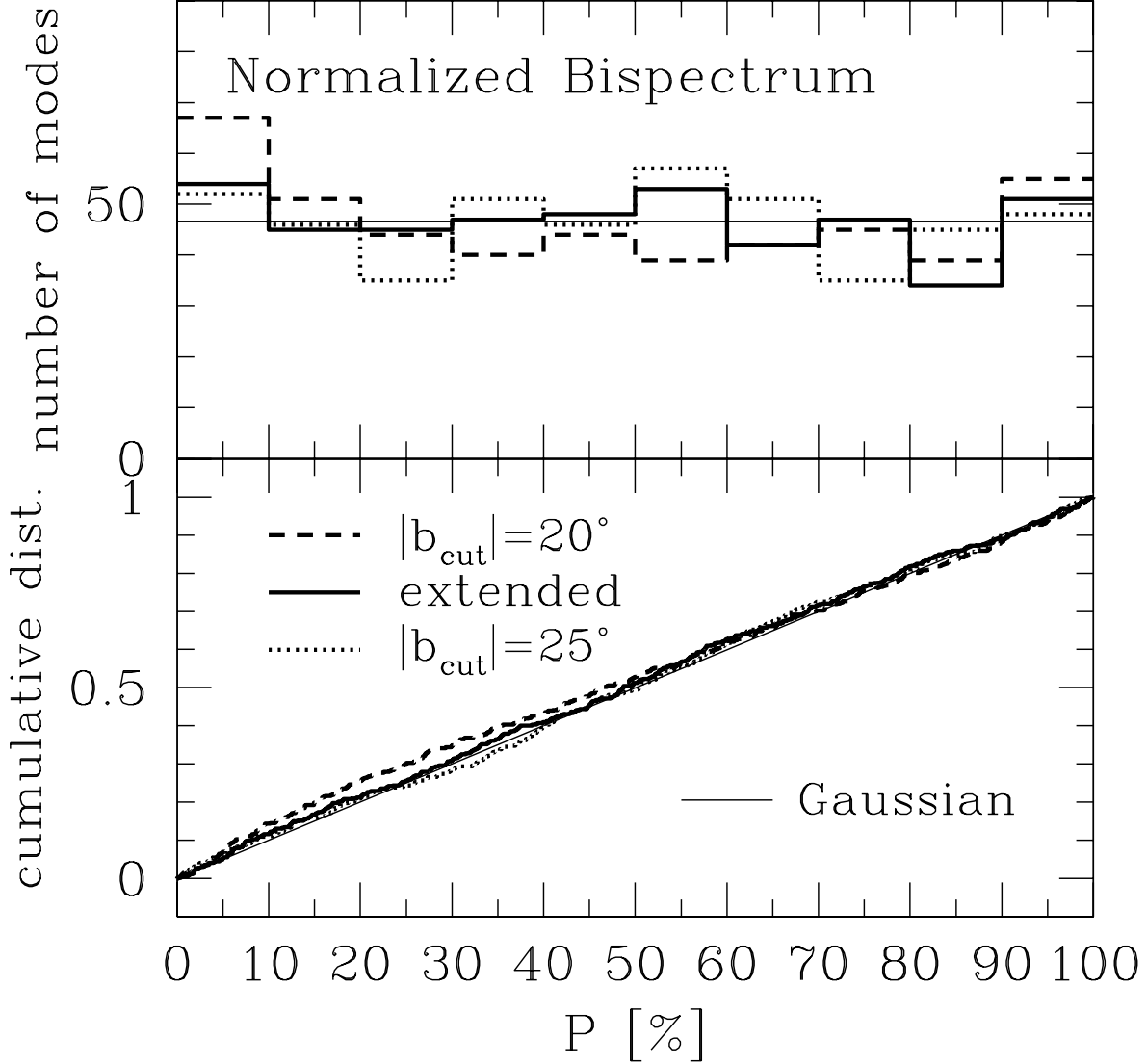


Fig. 4.— P distribution (Eq.(8)). P is the probability of the CMB normalized bispectrum, $B_{l_1 l_2 l_3} / (C_{l_1} C_{l_2} C_{l_3})^{1/2}$, measured on the *COBE* DMR 53 + 90 GHz sky map, being larger than those drawn from the Monte–Carlo simulations. There are 466 modes in total. The thick dashed, solid, and dotted lines represent the three different Galactic cuts as quoted in the figure. The thin solid line shows the expectation value for a Gaussian field. The top panel shows the P distribution, while the bottom panel shows the cumulative P distribution, for which we calculate the KS statistic. The KS statistic gives the probability of the distribution being consistent with the expectation for Gaussianity as 6.7%, 73%, and 77% for the three Galactic cuts, respectively.

4.1. Primary bispectrum

For the primary bispectrum from inflation, we consider weakly non-Gaussian adiabatic perturbations generated through non-linearity in slow-roll inflation. The simplest weak non-linear coupling gives

$$\Phi(\mathbf{x}) = \Phi_L(\mathbf{x}) + f_{\text{NL}} [\Phi_L^2(\mathbf{x}) - \langle \Phi_L^2(\mathbf{x}) \rangle], \quad (10)$$

where the square bracket denotes the volume average, and $\Phi_L(\mathbf{x})$ is a linear Gaussian part of curvature perturbations. We call f_{NL} the non-linear coupling parameter, following Komatsu and Spergel (2001).

Salopek and Bond (1990, 1991) and Gangui et al. (1994) show that slow-roll inflation gives this coupling; Pyne and Carroll (1996) shows that the second-order general relativistic perturbation theory gives this. The former predicts f_{NL} as a certain combination of slope and curvature of a inflaton potential ($\Phi_3 = -2f_{\text{NL}}$ in Gangui et al. (1994); $\alpha_\Phi = f_{\text{NL}}$ in Verde et al. (2000)). The latter predicts $f_{\text{NL}} \sim \mathcal{O}(1)$. Komatsu and Spergel (2001) have given the exact form of $B_{l_1 l_2 l_3}$ for this model; we do not repeat it here. f_{NL} is the parameter that we try to constrain by measuring the CMB bispectrum.

Since the theoretical bispectrum assumes full sky coverage, we must correct it for the bias arising from incomplete sky coverage. We use an approximate correction factor for the bias, $\Omega_{\text{obs}}/4\pi$, which we have derived in the appendix. Moreover, the theoretical bispectrum must also be convolved with the DMR beam. We use the harmonic transform of the DMR beam, G_l , given in Wright et al. (1994). Hence, we relate the observed bispectrum to the theoretical bispectrum through

$$B_{l_1 l_2 l_3}^{\text{obs}} = \frac{\Omega_{\text{obs}}}{4\pi} B_{l_1 l_2 l_3}^{\text{theory}} G_{l_1} G_{l_2} G_{l_3}. \quad (11)$$

Note that $\Omega_{\text{obs}}/4\pi = 1 - \sin |b_{\text{cut}}|$ for an azimuthally symmetric cut within certain latitude b_{cut} ; $\Omega_{\text{obs}}/4\pi = 0.658$, 0.577 , and 0.5 for $|b_{\text{cut}}| = 20^\circ$, 25° , and 30° , respectively. For the extended cut, $\Omega_{\text{obs}}/4\pi = 0.638$.

4.2. Foreground bispectra from interstellar emissions

Although we cut a fraction of the sky to reduce interstellar emissions from the Galactic plane, there should be some residuals at high Galactic latitude. Kogut et al. (1996a) have found significant correlation between *COBE* DMR maps at high Galactic latitude and *COBE* Diffuse Infrared Background Experiment (DIRBE) map which mainly trace dust emission from the Galactic plane.

The interstellar emissions are highly non-Gaussian. For example, the one-point p.d.f of the all-sky dust template map (Schlegel et al. 1998) is highly skewed. We find the normalized skewness, $\langle (\Delta T)^3 \rangle / \langle (\Delta T)^2 \rangle^{3/2} \sim 51$. Since these non-Gaussian emissions would confuse the parameter estimation of the primary CMB bispectrum, we take the effect into account.

We estimate the foreground bispectra from interstellar sources by using two foreground template maps. One is the dust template map of Schlegel et al. (1998); the other is the synchrotron map of Haslam et al. (1981). Both maps are in the HEALPix format (Górski et al. 1998).

We extrapolate the dust map to 53 GHz and 90 GHz with taking into account spatial variations of dust temperatures across the sky (Finkbeiner et al. 1999). We then cross-correlate the extrapolated maps with the DMR maps to confirm that the extrapolation is reasonable. We find that while the dust-correlated emission in the DMR 90 GHz map is consistent with the extrapolated dust emission, that in the DMR 53 GHz map is much larger than the extrapolated one. This is consistent with the anomalous microwave emission of Kogut et al. (1996a). To take the excess emission into account, we multiply our extrapolated 53 GHz maps by factors of 3.66, 2.58, and 2.59 for the 20° cut, the extended cut, and the 25° cut, respectively. The correction factor is notably larger for the 20° cut rather than the extended or 25° cut. This could possibly be attributed to the region around Ophiucus which has a free-free spectrum. Note that we do not essentially need the correction for the excess emission, as it does not alter spatial distribution of the emission. Nevertheless, we do it for convenience of subsequent analyses.

We also extrapolate the synchrotron map to these two bands, assuming the spectrum of the source, $T(\nu) \propto \nu^{-2.9}$. We do not need the extrapolation of the synchrotron template map either, as the extrapolation does not alter spatial distribution of the emission in contrast to the dust template map in which the extrapolation does alter it. We find no significant correlation between the DMR maps and the extrapolated synchrotron maps at both 53 GHz and 90 GHz.

After coadding the extrapolated 53 and 90 GHz maps with the same weight as used for the DMR maps, we measure $B_{l_1 l_2 l_3}$ from the maps for the three different Galactic cuts, multiplying it by $G_{l_1} G_{l_2} G_{l_3}$ to take into account the DMR beam.

4.3. Constraints on non-linearity in inflation

We fit simultaneously the primary, dust, and synchrotron bispectra to the measured bispectrum on the DMR map. We use the least-squares method based on a χ^2 statistic defined by

$$\chi^2(f_j) \equiv \sum_{\alpha\alpha'} \left(I_{\alpha}^{\text{DMR}} - \sum_j f_j I_{\alpha}^j \right) (C^{-1})_{\alpha\alpha'} \left(I_{\alpha'}^{\text{DMR}} - \sum_j f_j I_{\alpha'}^j \right). \quad (12)$$

I_{α}^j is a model bispectrum divided by $(\langle C_{l_1}^{\text{MC}} \rangle \langle C_{l_2}^{\text{MC}} \rangle \langle C_{l_3}^{\text{MC}} \rangle)^{1/2}$, where j represents a certain component such as the primary, dust, and synchrotron. f_j is a fitting parameter for a component j , where $f_{\text{primary}} \equiv f_{\text{NL}}$ is the non-linear coupling parameter (Eq.(10)). f_{dust} and f_{sync} characterize amplitude of the foreground bispectra.

$C_{\alpha\alpha'}$ is the covariance matrix of the normalized bispectrum, which we calculate from the

Monte–Carlo simulations:

$$C_{\alpha\alpha'} \equiv \frac{1}{N-1} \sum_{i=1}^N \left(I_{\alpha}^{\text{MC}(i)} - \langle I_{\alpha}^{\text{MC}} \rangle \right) \left(I_{\alpha'}^{\text{MC}(i)} - \langle I_{\alpha'}^{\text{MC}} \rangle \right), \quad (13)$$

where $N = 50,000$ is the total number of realizations. The bracket denotes an average over all realizations, $\langle I_{\alpha}^{\text{MC}} \rangle \equiv N^{-1} \sum_i I_{\alpha}^{\text{MC}(i)}$. Here, we have implicitly assumed the non-Gaussianity weak, so that we calculate the covariance matrix from Gaussian realizations.

As we have observed in the previous section, distribution of I_{α} is very much Gaussian; thus, $\chi^2(f_j)$ should obey the χ^2 distribution to good accuracy. Hence, minimizing $\chi^2(f_j)$ with respect to f_j gives the maximum-likelihood value of f_j as a solution to the normal equation,

$$f_j = \sum_i (F^{-1})_{ji} \left[\sum_{\alpha\alpha'} I_{\alpha}^i (C^{-1})_{\alpha\alpha'} I_{\alpha'}^{\text{DMR}} \right], \quad (14)$$

where

$$F_{ij} \equiv \sum_{\alpha\alpha'} I_{\alpha}^i (C^{-1})_{\alpha\alpha'} I_{\alpha'}^j. \quad (15)$$

We estimate statistical uncertainties of the parameters using the Monte–Carlo simulations; we obtain parameter realizations by substituting I_{α}^{MC} for I_{α}^{DMR} in equation (14).

Figure 5 plots the measured values of the non-linear coupling parameter, f_{NL} , as well as the simulated realizations, for the three different Galactic cuts. The measured values are well within the cosmic variance: we place 68% confidence limits on f_{NL} as $|f_{\text{NL}}| < 1.6 \times 10^3$, 1.5×10^3 , and 1.7×10^3 , for the 20° cut, the extended cut, and the 25° cut, respectively.

Figures 6 and 7 plot constraints on f_{dust} and f_{sync} , respectively. There is no indication of either component contributing to the measured bispectrum significantly.

4.4. Null test of the normalized bispectrum

Using χ^2 defined by equation (12), we can test Gaussianity of the DMR map. While the minimization of $\chi^2(f_j)$ gives constraints on the parameters, a value of $\chi^2(f_j)$ tells us goodness-of-fit; $\chi^2(0)$ tests a hypothesis of the bispectrum being zero. When $\chi^2(0)$ is either significantly greater or smaller than those drawn from the simulations, we conclude that the DMR map is inconsistent with zero bispectrum.

$\chi^2(0)$ is similar to what several authors have used for quantifying statistical significance of non-Gaussianity in the DMR map (Ferreira et al. 1998; Magueijo 2000; Sandvik and Magueijo 2000). They use only diagonal terms of the covariance matrix; however, the matrix is diagonal only on the full sky. As lack of sky coverage correlates one mode to the others, we should include off-diagonal terms as well. We did so in equation (12).

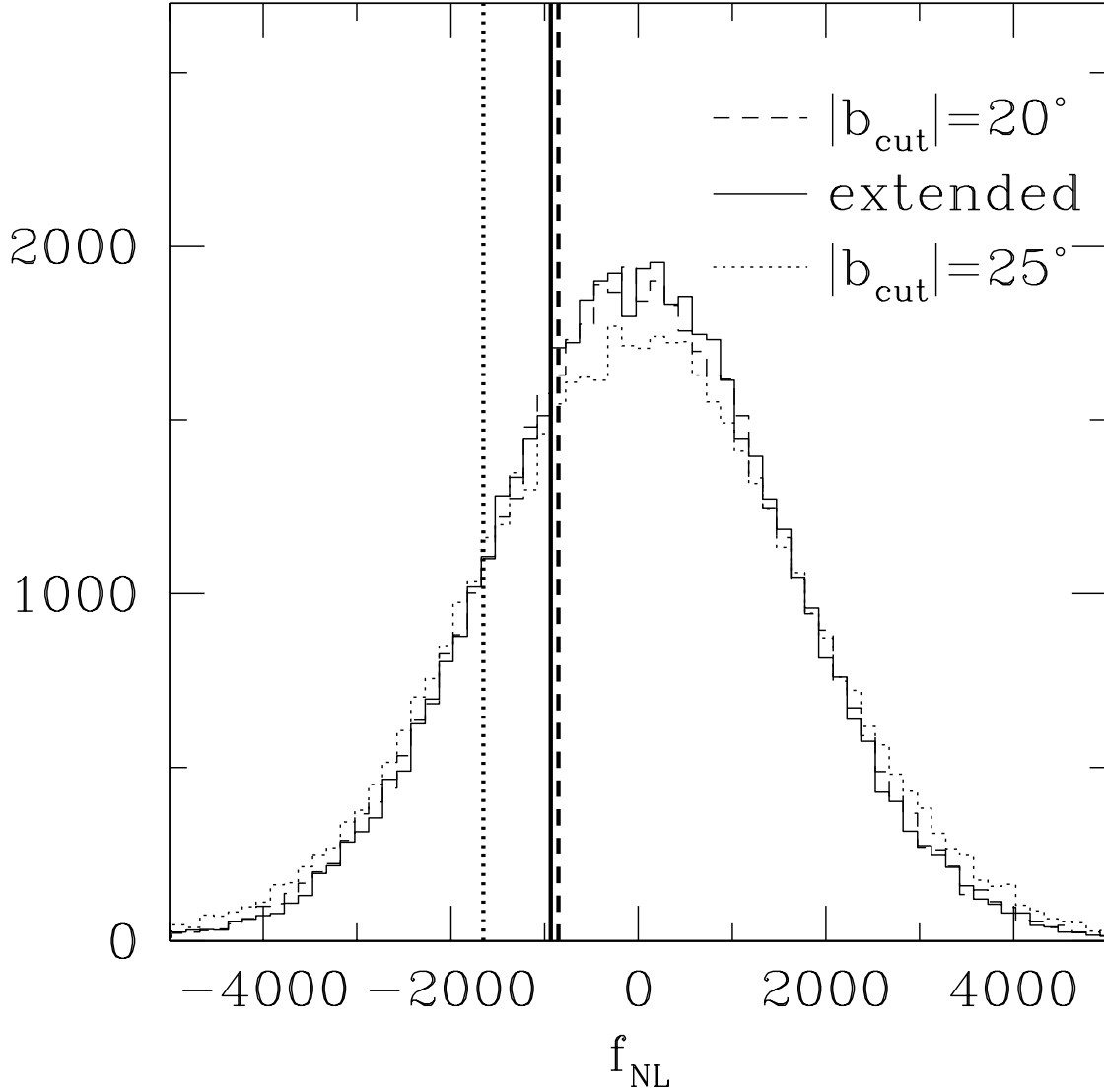


Fig. 5.— Constraint on the non-linear coupling parameter, f_{NL} , which characterizes non-linearity in inflation (Eq.(10)). The dashed, solid, and dotted lines represent the three different Galactic cuts as quoted in the figure. The thick vertical lines plot the measured values of f_{NL} from the *COBE* DMR maps, while the histograms plot those drawn from the Monte-Carlo simulations for each cut. 68% confidence limits on f_{NL} are $|f_{\text{NL}}| < 1.6 \times 10^3$, 1.5×10^3 , and 1.7×10^3 for the three cuts, respectively.

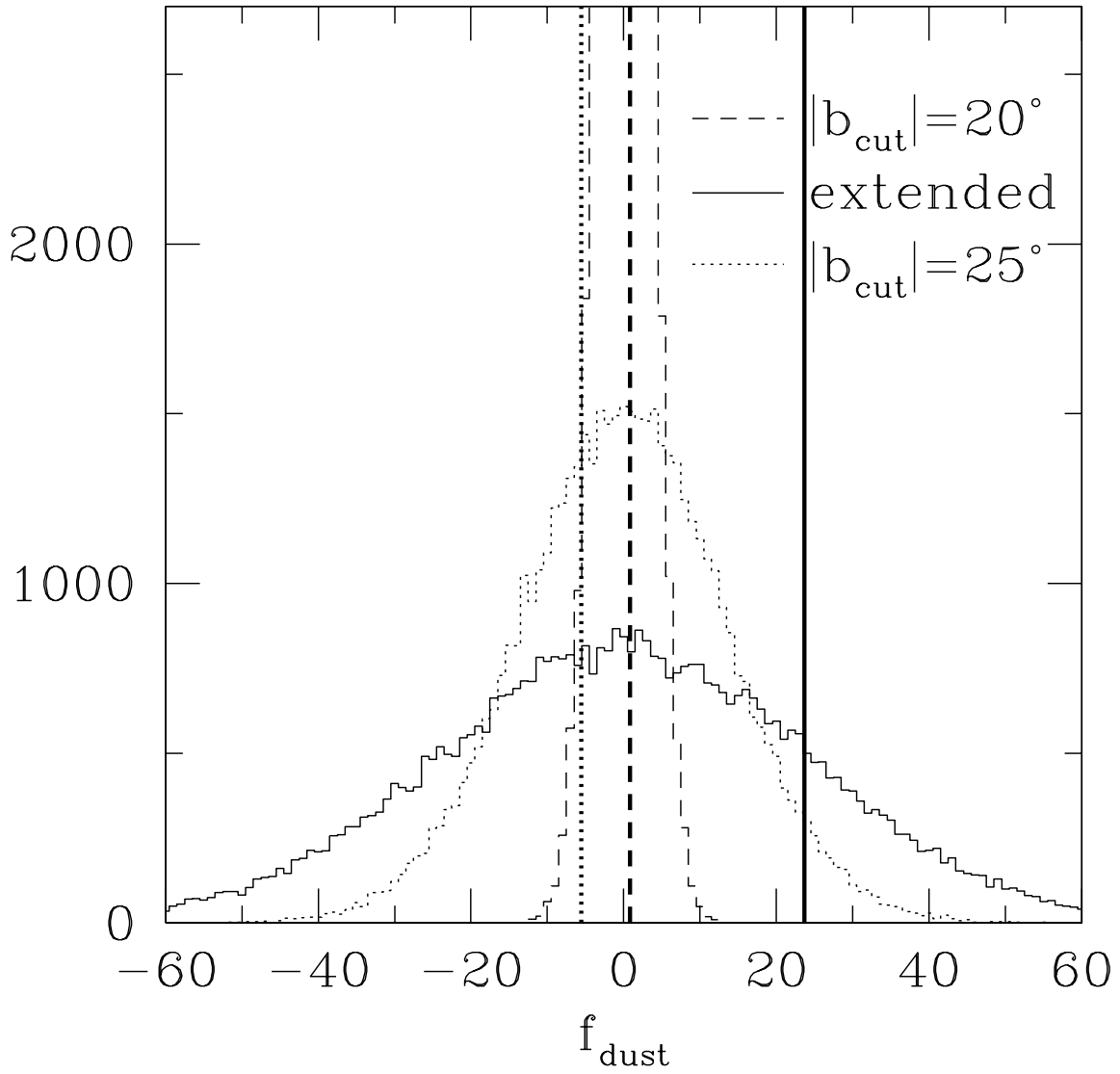


Fig. 6.— Constraint on amplitude of the interstellar dust bispectrum, f_{dust} . The meaning of the lines is the same as in figure 5.

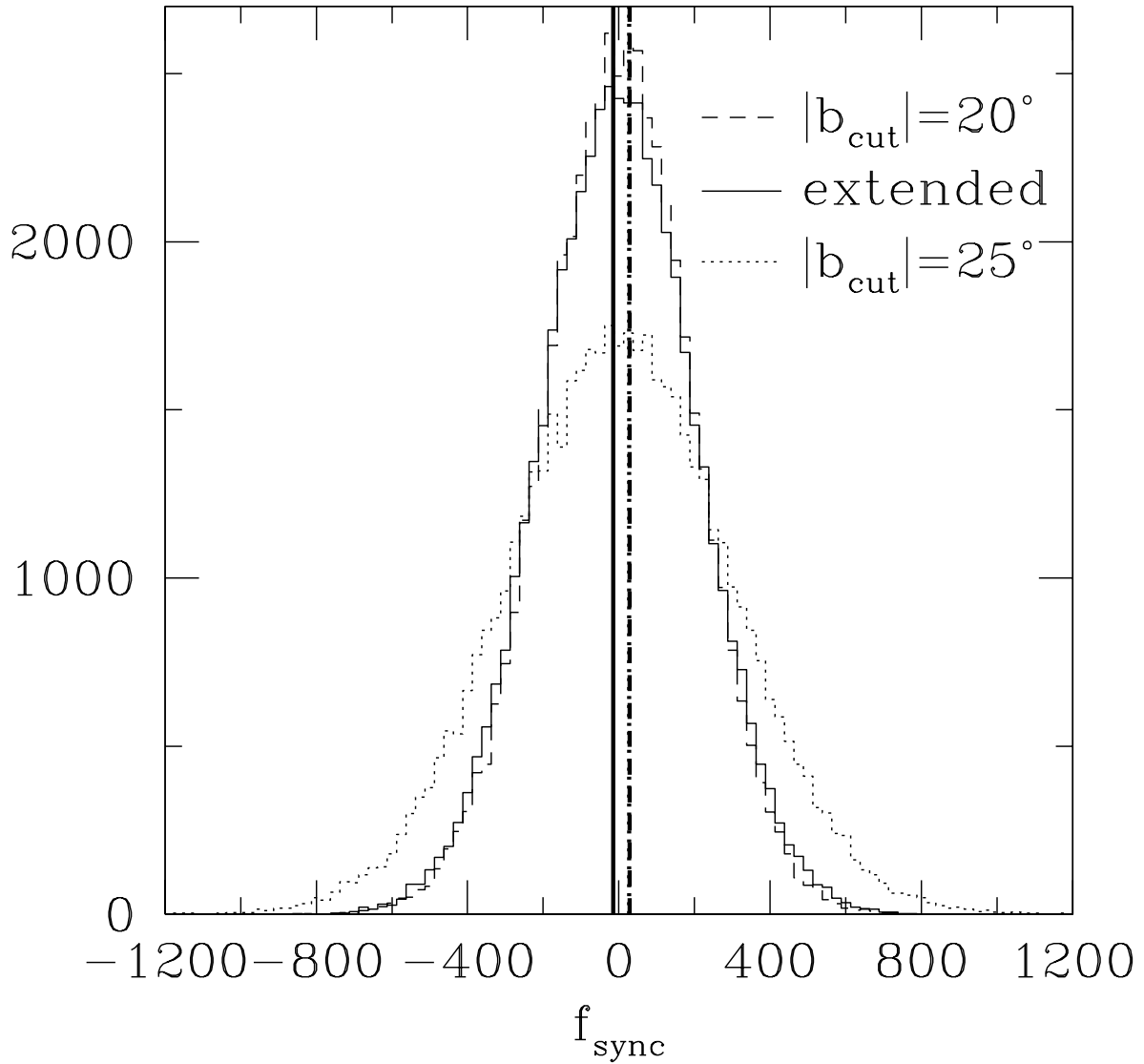


Fig. 7.— Constraint on amplitude of the interstellar synchrotron bispectrum, f_{sync} . The meaning of the lines is the same as in figure 5.

Figure 8 compares $\chi_{\text{DMR}}^2(0)$ with $\chi_{\text{MC}}^2(0)$ for the different Galactic cuts. The measured values are $\chi_{\text{DMR}}^2(0) = 475.6, 462.7,$ and 464.8 for the corresponding Galactic cuts, respectively, while $\langle \chi_{\text{MC}}^2(0) \rangle = 466$. We find the probability of $\chi_{\text{MC}}^2(0)$ being larger than $\chi_{\text{DMR}}^2(0)$ to be $P(\chi_{\text{MC}}^2 > \chi_{\text{DMR}}^2) = 36.9\%, 47.0\%,$ and 49.7% , respectively.

We conclude that the DMR map is comfortably consistent with zero normalized bispectrum. We explain the claimed detection (Ferreira et al. 1998) by a statistical fluctuation as an alternative to the "eclipse effect" proposition made in Banday et al. (2000).

There is no evidence that the scatter of the normalized bispectrum is too small to be consistent with Gaussian, in contrast to the claim of Magueijo (2000) based on $\chi^2(0)$ derived from 8 modes. To clarify, our analysis does not reject the possibility that the CMB sky is non-Gaussian for only a small number of modes; however, in the absence of a theoretical motivation for limiting the analysis to a specific set of modes, we choose to treat all the bispectrum modes on an equal footing. Sandvik and Magueijo (2000) claim that the non-Gaussianity found by Magueijo (2000) does not spread to other modes. This is consistent with our result.

Incidentally, we plot in the figure 8 the χ^2 distribution for 466 degrees of freedom, χ_{466}^2 , in filled circles; we find that the distribution of $\chi_{\text{MC}}^2(0)$ is very similar to the χ_{466}^2 distribution for a smaller cut as expected, while it becomes slightly broader for a larger cut for which the distribution of the normalized bispectrum deviates from Gaussian appreciably. Yet, we find that the $20^\circ - 25^\circ$ cuts reasonably retain the Gaussianity of the distribution of the normalized bispectrum.

5. DISCUSSION AND CONCLUSIONS

In this paper, we have measured all independent configurations of the angular bispectrum on the *COBE* DMR map, down to the DMR beam size. Using the most sensitive sky map to CMB, which combines the maps at 53 and 90 GHz, we test the Gaussianity of the DMR map.

We find that the normalized bispectrum, $B_{l_1 l_2 l_3} / (C_{l_1} C_{l_2} C_{l_3})^{1/2}$, gives more robust test of Gaussianity than the bare bispectrum, $B_{l_1 l_2 l_3}$. We compare the measured data with the simulated realizations, finding the DMR map comfortably consistent with Gaussian. We explain the reported detection of the normalized bispectrum at $l_1 = l_2 = l_3 = 16$ (Ferreira et al. 1998) by a statistical fluctuation. While it is still conceivable that the eclipse effect of the Earth against the *COBE* satellite generates some of the bispectrum (Banday et al. 2000), the DMR data cannot distinguish it from the statistical fluctuations.

We fit the predicted bispectra to the data, constraining the parameters in the predictions, which include the primary bispectrum from inflation and the foreground bispectra from interstellar dust and synchrotron emissions. We find that neither dust nor synchrotron emissions contribute to the bispectrum significantly.

We have obtained a weak constraint on the non-linear coupling parameter, f_{NL} , that charac-

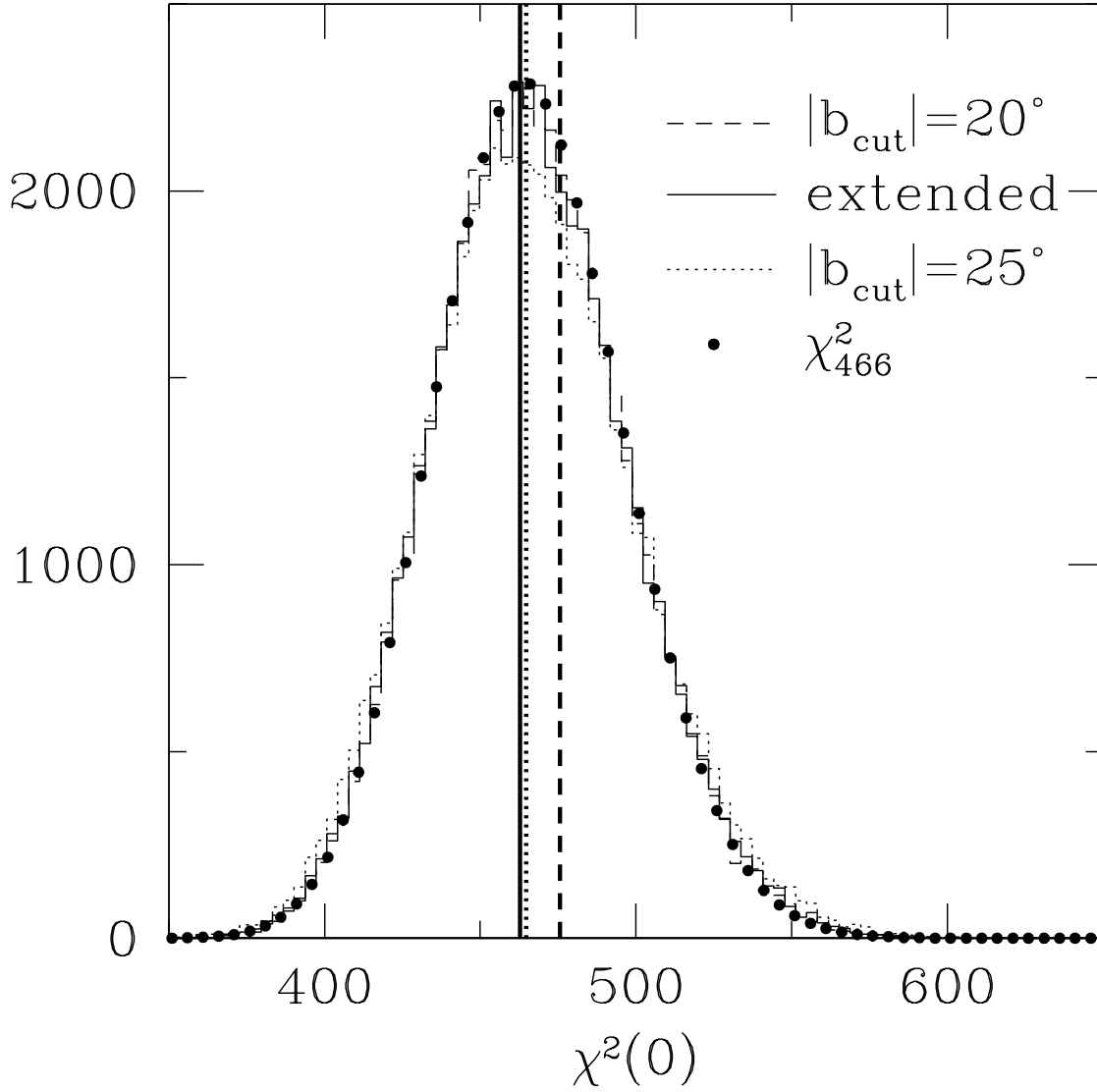


Fig. 8.— Testing hypothesis of the normalized bispectrum, $B_{l_1 l_2 l_3} / (C_{l_1} C_{l_2} C_{l_3})^{1/2}$, being zero in the *COBE* DMR four-year 53 + 90 GHz sky map. The dashed, solid, and dotted lines represent the 20° cut, the extended cut, and the 25° cut, respectively. The thick vertical lines plot the measured $\chi^2(0)$, while the histograms plot those drawn from the Monte-Carlo simulations. The filled circles plot the χ^2 distribution for 466 degrees of freedom.

terizes non-linearity in inflation. We interpret the constraint in terms of a single field inflation as follows. According to the analysis of non-linear perturbations on super horizon scales (Salopek and Bond 1990), we can explicitly calculate f_{NL} as

$$f_{\text{NL}} = -\frac{5}{24\pi G} \left(\frac{\partial^2 \ln H}{\partial \phi^2} \right), \quad (16)$$

where H is the Hubble parameter during inflation. When applying the slow-roll conditions to an inflaton potential $V(\phi)$, we have $\partial \ln H / \partial \phi \approx (d \ln V / d\phi) / 2$; thus, f_{NL} is on the order of curvature of a slow-roll potential, implying that $|f_{\text{NL}}|$ should be smaller than 1 in slow-roll inflation. Therefore, the obtained constraint, $|f_{\text{NL}}| < 1.5 \times 10^3$, seems too weak to be interesting; however, any deviation from slow-roll could yield larger $|f_{\text{NL}}|$, bigger non-Gaussianity.

The next generation satellite experiments, the *Microwave Anisotropy Probe (MAP)* and *Planck*, should be able to put more stringent constraints on f_{NL} . Komatsu and Spergel (2001) have shown that *MAP* and *Planck* should be sensitive down to $|f_{\text{NL}}| \sim 20$ and 5, respectively. We find that the actual constraint from *COBE* (figure 5) is much worse than the estimate. This is partly due to different cosmology used for the model, but mainly due to incomplete sky coverage; the statistical power of the bispectrum at low multipoles is significantly weakened by the Galactic cut. Since *MAP* and *Planck* probe much smaller angular scales, and their better angular resolution makes an extent of the Galactic cut smaller, the degradation of sensitivity should be minimal. Moreover, the improved frequency coverage of future experiments will aid in extracting more usable CMB pixels from the data. At this level of sensitivity, any deviation from slow-roll could give an interesting amount of the bispectrum, and *MAP* and *Planck* will put severe constraints on any substantial deviation from slow-roll.

While we have explored adiabatic generation of the bispectrum only, isocurvature perturbations from inflation also generate non-Gaussianity (Linde and Mukhanov 1997; Peebles 1997; Bucher and Zhu 1997). They are in general more non-Gaussian than the adiabatic perturbations; it is worth constraining those models by the same strategy as we have done in this paper.

We would like to thank Charles L. Bennett, Gary Hinshaw, Misao Sasaki, Licia Verde, and Edward L. Wright for helpful discussions. We would like to thank Uroš Seljak and Matias Zaldarriaga for making their CMBFAST code publicly available. E. K. acknowledges financial support from the Japan Society for the Promotion of Sciences. D. N. S. and B. D. W. are partially supported by the MAP/MIDEX program.

A. ANGULAR POWER SPECTRUM AND BISPECTRUM ON THE INCOMPLETE SKY

Incomplete sky coverage destroys orthonormality of the spherical harmonics on the sky. The degree to which orthonormality is broken is often characterized by the coupling integral (Peebles

1980),

$$W_{ll'mm'} \equiv \int d^2\hat{\mathbf{n}} W(\hat{\mathbf{n}}) Y_{lm}^*(\hat{\mathbf{n}}) Y_{l'm'}(\hat{\mathbf{n}}) = \int_{\Omega_{\text{obs}}} d^2\hat{\mathbf{n}} Y_{lm}^*(\hat{\mathbf{n}}) Y_{l'm'}(\hat{\mathbf{n}}), \quad (\text{A1})$$

where $W(\hat{\mathbf{n}})$ is zero in a cut region otherwise 1, and Ω_{obs} denotes a solid angle of the observed sky. When $W_{ll'mm'} \neq \delta_{ll'}\delta_{mm'}$, the measured harmonic transform of the temperature anisotropy field, a_{lm} , becomes a *biased* estimator of the true harmonic transform, a_{lm}^{true} , through

$$a_{lm} = \sum_{l'=0}^{\infty} \sum_{m'=-l'}^{l'} a_{l'm'}^{\text{true}} W_{ll'mm'}. \quad (\text{A2})$$

Hence, we must correct our estimators of the power spectrum and the bispectrum for the bias arising from incomplete sky coverage.

First, we derive a relationship between the angular power spectrum on the incomplete sky and that on the full sky. Taking the ensemble average of the estimator of the power spectrum, the pseudo- C_l (Wandelt et al. 1998, 2000), $C_l = (2l+1)^{-1} \sum_m |a_{lm}|^2$, we have

$$\begin{aligned} \langle C_l \rangle &= \frac{1}{2l+1} \sum_{l'} C_{l'}^{\text{true}} \sum_{mm'} |W_{ll'mm'}|^2 \\ &\approx \frac{1}{2l+1} C_l^{\text{true}} \sum_m \sum_{l'm'} \int d^2\hat{\mathbf{n}} W(\hat{\mathbf{n}}) Y_{lm}^*(\hat{\mathbf{n}}) Y_{l'm'}(\hat{\mathbf{n}}) \int d^2\hat{\mathbf{m}} W(\hat{\mathbf{m}}) Y_{lm}(\hat{\mathbf{m}}) Y_{l'm'}^*(\hat{\mathbf{m}}) \\ &= \frac{1}{2l+1} C_l^{\text{true}} \sum_m \int d^2\hat{\mathbf{n}} W(\hat{\mathbf{n}}) Y_{lm}^*(\hat{\mathbf{n}}) \int d^2\hat{\mathbf{m}} W(\hat{\mathbf{m}}) Y_{lm}(\hat{\mathbf{m}}) \delta^{(2)}(\hat{\mathbf{n}} - \hat{\mathbf{m}}) \\ &= C_l^{\text{true}} \int \frac{d^2\hat{\mathbf{n}}}{4\pi} W(\hat{\mathbf{n}}) P_l(1) \\ &= C_l^{\text{true}} \frac{\Omega_{\text{obs}}}{4\pi}. \end{aligned} \quad (\text{A3})$$

In the second equality, we have taken $C_{l'}^{\text{true}}$ out of the summation over l' , as $|W_{ll'mm'}|^2$ peaks very sharply at $l = l'$, and $C_{l'}^{\text{true}}$ varies much more slowly than $|W_{ll'mm'}|^2$ in l' . This approximation is good for nearly full sky coverage. In the third equality, we have used $\sum_{l'm'} Y_{l'm'}(\hat{\mathbf{n}}) Y_{l'm'}^*(\hat{\mathbf{m}}) = \delta^{(2)}(\hat{\mathbf{n}} - \hat{\mathbf{m}})$. In the fourth equality, we have used $\sum_m Y_{lm}^*(\hat{\mathbf{n}}) Y_{lm}(\hat{\mathbf{m}}) = \frac{2l+1}{4\pi} P_l(\hat{\mathbf{n}} \cdot \hat{\mathbf{m}})$. The result indicates that the bias amounts approximately to a fraction of the sky covered by observations.

Next, we derive a relationship between the angular bispectrum on the incomplete sky and that on the full sky. We begin with

$$\langle a_{l_1 m_1} a_{l_2 m_2} a_{l_3 m_3} \rangle = \sum_{\text{all } l'm'} \left\langle a_{l_1 m_1}^{\text{true}} a_{l_2 m_2}^{\text{true}} a_{l_3 m_3}^{\text{true}} \right\rangle W_{l_1 l_1' m_1 m_1'} W_{l_2 l_2' m_2 m_2'} W_{l_3 l_3' m_3 m_3'}. \quad (\text{A4})$$

Rotational and parity invariance of the bispectrum implies the bispectrum given by

$$\langle a_{l_1 m_1} a_{l_2 m_2} a_{l_3 m_3} \rangle = b_{l_1 l_2 l_3} \int d^2\hat{\mathbf{n}} Y_{l_1 m_1}^*(\hat{\mathbf{n}}) Y_{l_2 m_2}^*(\hat{\mathbf{n}}) Y_{l_3 m_3}^*(\hat{\mathbf{n}}), \quad (\text{A5})$$

where $b_{l_1 l_2 l_3}$ is an arbitrary real symmetric function, which is related to the angular averaged bispectrum, $B_{l_1 l_2 l_3}$. When $b_{l_1 l_2 l_3}^{\text{true}}$ varies much more slowly than the coupling integral, we obtain

$$\begin{aligned}
\langle a_{l_1 m_1} a_{l_2 m_2} a_{l_3 m_3} \rangle &= \sum_{\text{all } l'} b_{l'_1 l'_2 l'_3}^{\text{true}} \sum_{\text{all } m'} \int d^2 \hat{\mathbf{n}} Y_{l'_1 m'_1}^* (\hat{\mathbf{n}}) Y_{l'_2 m'_2}^* (\hat{\mathbf{n}}) Y_{l'_3 m'_3}^* (\hat{\mathbf{n}}) \\
&\times \int d^2 \hat{\mathbf{n}}_1 W(\hat{\mathbf{n}}_1) Y_{l'_1 m'_1} (\hat{\mathbf{n}}_1) Y_{l_1 m_1}^* (\hat{\mathbf{n}}_1) \\
&\times \int d^2 \hat{\mathbf{n}}_2 W(\hat{\mathbf{n}}_2) Y_{l'_2 m'_2} (\hat{\mathbf{n}}_2) Y_{l_2 m_2}^* (\hat{\mathbf{n}}_2) \\
&\times \int d^2 \hat{\mathbf{n}}_3 W(\hat{\mathbf{n}}_3) Y_{l'_3 m'_3} (\hat{\mathbf{n}}_3) Y_{l_3 m_3}^* (\hat{\mathbf{n}}_3) \\
&\approx b_{l_1 l_2 l_3}^{\text{true}} \int d^2 \hat{\mathbf{n}} W(\hat{\mathbf{n}}) Y_{l_1 m_1}^* (\hat{\mathbf{n}}) Y_{l_2 m_2}^* (\hat{\mathbf{n}}) Y_{l_3 m_3}^* (\hat{\mathbf{n}}). \tag{A6}
\end{aligned}$$

Then, we calculate the angular averaged bispectrum, $B_{l_1 l_2 l_3}$ (Eq.(1)). By convolving equation (A6) with the Wigner-3j symbol and using the identity (3), we obtain

$$\begin{aligned}
\langle B_{l_1 l_2 l_3} \rangle &\approx b_{l_1 l_2 l_3}^{\text{true}} \sqrt{\frac{4\pi}{(2l_1 + 1)(2l_2 + 1)(2l_3 + 1)}} \begin{pmatrix} l_1 & l_2 & l_3 \\ 0 & 0 & 0 \end{pmatrix}^{-1} \\
&\times \sum_{\text{all } m} \int d^2 \hat{\mathbf{m}} Y_{l_1 m_1} (\hat{\mathbf{m}}) Y_{l_2 m_2} (\hat{\mathbf{m}}) Y_{l_3 m_3} (\hat{\mathbf{m}}) \\
&\times \int d^2 \hat{\mathbf{n}} W(\hat{\mathbf{n}}) Y_{l_1 m_1}^* (\hat{\mathbf{n}}) Y_{l_2 m_2}^* (\hat{\mathbf{n}}) Y_{l_3 m_3}^* (\hat{\mathbf{n}}) \\
&= b_{l_1 l_2 l_3}^{\text{true}} \sqrt{\frac{(2l_1 + 1)(2l_2 + 1)(2l_3 + 1)}{4\pi}} \begin{pmatrix} l_1 & l_2 & l_3 \\ 0 & 0 & 0 \end{pmatrix}^{-1} \\
&\times \int \frac{d^2 \hat{\mathbf{m}}}{4\pi} \int \frac{d^2 \hat{\mathbf{n}}}{4\pi} W(\hat{\mathbf{n}}) P_{l_1}(\hat{\mathbf{m}} \cdot \hat{\mathbf{n}}) P_{l_2}(\hat{\mathbf{m}} \cdot \hat{\mathbf{n}}) P_{l_3}(\hat{\mathbf{m}} \cdot \hat{\mathbf{n}}) \\
&= b_{l_1 l_2 l_3}^{\text{true}} \sqrt{\frac{(2l_1 + 1)(2l_2 + 1)(2l_3 + 1)}{4\pi}} \begin{pmatrix} l_1 & l_2 & l_3 \\ 0 & 0 & 0 \end{pmatrix} \frac{\Omega_{\text{obs}}}{4\pi} \\
&= B_{l_1 l_2 l_3}^{\text{true}} \frac{\Omega_{\text{obs}}}{4\pi}, \tag{A7}
\end{aligned}$$

where we have used the identity,

$$\int_{-1}^1 \frac{dx}{2} P_{l_1}(x) P_{l_2}(x) P_{l_3}(x) = \begin{pmatrix} l_1 & l_2 & l_3 \\ 0 & 0 & 0 \end{pmatrix}^2. \tag{A8}$$

Thus, the bias for the angular bispectrum on the incomplete sky is also approximately given by a fraction of the sky covered by observations.

REFERENCES

Albrecht, A., and Steinhardt, P. J. 1982, Phys. Rev. Lett., 48, 1220

- Banday, A. J., Górski, K. M., Bennett, C. L., Hinshaw, G., Kogut, A., Lineweaver, C., Smoot, G. F., and Tenorio, L. 1997, *ApJ*, 475, 393
- Banday, A. J., Zaroubi, S., and Górski, K. M. 2000, *ApJ*, 533, 575
- Bardeen, J. M., Steinhardt, P. J., and Turner, M. S. 1983, *Phys. Rev. D*, 28, 679
- Bennett, C. L., et al. 1996, *ApJ*, 464, L1
- Bucher, M., and Zhu, Y. 1997, *Phys. Rev. D*, 55, 7415
- de Bernardis, P., et al. 2000, *Nature*, 404, 955
- Bromley, B. C., and Tegmark, M. 1999, *ApJ*, 524, L79
- Bunn, E. F., and White, M. 1997, *ApJ*, 480, 6
- Cooray, A., and Hu, W. 2000, *ApJ*, 534, 533
- Falk, T., Rangarajan, R., Srednicki, M. 1993, *ApJ*, 403, L1
- Ferreira, P. G., Magueijo, J., and Górski, K. M. 1998, *ApJ*, 503, L1
- Finkbeiner, D. P., Davis, M., and Schlegel, D. J., 1999, *ApJ*, 524, 867
- Gangui, A., Lucchin, F., Matarrese, S., and Mollerach, S. 1994, *ApJ*, 430, 447
- Gangui, A., and Martin, J. 2000, *Phys. Rev. D*, 62, 103004
- Goldberg, D. M., and Spergel, D. N. 1999, *Phys. Rev. D*, 59, 103002
- Górski, K. M., Hivon, F., and Wandelt, B. D. 1998, in *Proceedings of the MPA/ESO Conference on Evolution of Large-Scale Structure: from Recombination to Garching*, edited by Banday, A. J., Sheth, R. K., and da Costa, L. N.
- Guth, A. 1981, *Phys. Rev. D*, 23, 347
- Guth, A., and Pi, S. Y. 1982, *Phys. Rev. Lett.*, 49, 1110
- Hanany, S., et al. 2000, *ApJ*, 545, L5
- Haslam, C. G. T., Klein, U., Salter, C. J., Stoffel, H., Wilson, W. E., Cleary, M. N., Cooke, D. J., Thomasson, P. 1981, *A&A*, 100, 209
- Hawking, S. 1982, *Phys. Lett.*, 115B, 295
- Heavens, A. F. 1998, *MNRAS*, 299, 805
- Kogut, A., Banday, A. J., Bennett, C. L., Górski, K. M., Hinshaw, G., Smoot, G. F., and Wright, E. L. 1996a, *ApJ*, 464, L5

- Kogut, A., Banday, A. J., Bennett, C. L., Górski, K. M., Hinshaw, G., Smoot, G. F., and Wright, E. L. 1996b, *ApJ*, 464, L29
- Komatsu, E., and Spergel, D. N. 2001, *Phys. Rev. D*, 63, 063002
- Linde, A. D. 1982, *Phys. Lett.*, 108B, 389
- Linde, A. D., and Mukhanov, V. 1997, *Phys. Rev. D*, 56, R535
- Lineweaver, C. H., et al. 1994, *ApJ*, 436, 452
- Luo, X., and Schramm, D. N. 1993, *Phys. Rev. Lett.*, 71, 1124
- Luo, X. 1994, *ApJ*, 427, L71
- Magueijo, J. 1995, *Phys. Lett.*, 342B, 32
- Magueijo, J. 2000, *ApJ*, 528, L57
- Miller A. D., et al. 1999, *ApJ*, 524, L1
- Peebles, P. J. E. 1980, *The Large-Scale Structure of the Universe*, Princeton University Press, Princeton
- Peebles, P. J. E. 1997, *ApJ*, 483, L1
- Phillips, N. G., and Kogut, A. 2001, *ApJ*, 548, 540
- Pyne, T., and Carroll, S. M. 1996, *Phys. Rev. D*, 53, 2920
- Salopek, D. S., and Bond, J. R. 1990, *Phys. Rev. D*, 42, 3936
- Salopek, D. S., and Bond, J. R. 1991, *Phys. Rev. D*, 43, 1005
- Sandvik, H. B., and Magueijo, J. 2000, preprint (astro-ph/0010395)
- Sato, K. 1981, *Phys. Lett.*, 99B, 66
- Schlegel, D. J., Finkbeiner, D. P., and Davis, M. 1998, *ApJ*, 500, 525
- Seljak, U., and Zaldarriaga, M. 1996, *ApJ*, 469, 437
- Spergel, D. N., and Goldberg, D. M. 1999, *Phys. Rev. D*, 59, 103001
- Starobinsky, A. A. 1982, *Phys. Lett.*, 117B, 175
- Verde, L., Wang, L., Heavens, A. F., and Kamionkowski, M. 2000, *MNRAS*, 313, 141
- Wandelt, B. D., Górski, K. M., and Hivon, E. 1998, preprint (astro-ph/9808292)

Wandelt, B. D., Hivon, E., and Górski, K. M. 2000, Phys. Rev. D, in press (astro-ph/0008111)

Wright, E. L., Smoot, G. F., Kogut, A., Hinshaw, G., Tenorio, L., Lineweaver, C., Bennett, C. L.,
and Lubin, P. M. 1994, ApJ, 420, 1